ISPRS Journal of Photogrammetry and Remote Sensing 105 (2015) 13–18

Contents lists available at ScienceDirect

ISPRS Journal of Photogrammetry and Remote Sensing

journal homepage: www.elsevier.com/locate/isprsjprs

Accurate direct georeferencing of aerial imagery in national coordinates ☆

Xiang Shen [a,b,c], Yongjun Zhang [b,*], Qingquan Li [a]

[a] Key Laboratory for Geo-Environment Monitoring of Coastal Zone of the National Administration of Surveying, Mapping and GeoInformation & Shenzhen Key Laboratory of Spatial Smart Sensing and Services, Shenzhen University, Nanhai Road 3688, Shenzhen 518060, PR China
[b] School of Remote Sensing and Information Engineering, Wuhan University, Luoyu Road 129, Wuhan 430079, PR China
[c] College of Information Engineering, Shenzhen University, Nanhai Road 3688, Shenzhen 518060, PR China

ARTICLE INFO

Article history:
Received 30 September 2014
Received in revised form 23 January 2015
Accepted 16 March 2015

Keywords:
Correction
Distortion
Georeferencing
Map projection

ABSTRACT

In aerial photogrammetry, data products are commonly needed in national coordinates, and, in practice, the georeferencing is often performed in the required national map projection frame directly. However, as a map projection frame is not Cartesian, some additional corrections are necessary in the georeferencing process to take account of various map projection distortions. This paper presents a new map projection correction method for the direct georeferencing of aerial images in national coordinates, which comprises of three consecutive steps: (1) a rough intersection to predict ground point coordinates in the Cartesian space; (2) calculating map projection corrections; and (3) a fine intersection. Benefiting from the explicit estimation of ground positions in the Cartesian space, our new method can directly adopt the accurate map projection distortion model that was previously developed for the direct georeferencing of airborne LiDAR data in national coordinates. Simulations show that the correction residuals of our new method are smaller by one order of magnitude than those of the previous best approach while their computational costs are at the same level, and even in an extreme scenario of 8000 m flight height above ground, the maximum error of our method is only several centimeters, which can be safely neglected in practical applications.

1. Introduction

Benefiting from the continuous improvement of GPS/INS hardware and integrated navigation technology, the exterior orientation parameters (EOPs) of aerial imagery can be directly and accurately acquired by an onboard position and orientation system (POS), and can be used for scene restitution directly (Yastikli and Jacobsen, 2005a; Legat, 2006). This georeferencing method, which is called direct georeferencing (DG), has gained increasing attention in the photogrammetry community because it does not need the field work of measuring ground control points and a bundle adjustment, and it can therefore greatly reduce data acquisition and processing costs (Skaloud, 2002; Cramer et al., 2012). However, as being an extrapolation method, DG is particularly sensitive to systematic and random errors (Yastikli and Jacobsen, 2005a,b).

Aerial photogrammetric products are typically needed in national coordinates and, accordingly, in practice, DG is often conducted in the required national frame directly (Zhang and Shen, 2013a). However, as a national frame is not Cartesian but rather defined by a national datum and a conformal map projection, the DG process in national coordinates is inevitably affected by a number of map projection distortions, which should be carefully corrected to acquire accurate DG results (Ressl, 2001; Yastikli and Jacobsen, 2005a,b; Legat, 2006; Zhang and Shen, 2013a,b).

Many map projection correction methods were developed for the DG of aerial imagery in national coordinates, and so far any of them was designed for correcting a specific distortion factor only (either the earth curvature distortion or length distortion. The earth curvature distortion and length distortion refer to the height difference and the horizontal length difference between a ground point and its corresponding projected point in the local level frame defined by the perspective center as the anchor point, respectively. The former is independent upon the map projection and the latter

☆ Most of this work was carried out while the first author was pursuing his doctoral degree at *School of Remote Sensing and Information Engineering, Wuhan University*.

* Corresponding author.
E-mail address: zhangyj@whu.edu.cn (Y. Zhang).

http://dx.doi.org/10.1016/j.isprsjprs.2015.03.008
0924-2716/

is not. For more details on the properties of these two distortion factors, please see Legat (2006), or Zhang and Shen (2013a)). To our best knowledge, all sophisticated earth curvature correction methods adopt a similar strategy that modifies image coordinates (Wang, 1990; Mikhail et al., 2001; Mugnier et al., 2004; Legat, 2006; Kraus, 2007; Zhao et al., 2014). The correction methods for the length distortion, on the other hand, are more diversified. Corrections can be added to flight heights (Ressl, 2001; Legat, 2006), focal lengths (Ressl, 2001; Yastikli and Jacobsen, 2005a,b), image coordinates (Zhang and Shen, 2013b), or ground heights (Zhang and Shen, 2013b).

Existing map projection correction methods were evaluated by a number of researchers using simulated (Legat, 2006; Zhang and Shen, 2013b; Zhao et al., 2014) or real data (Skaloud and Legat, 2008), and they were proven to be capable of substantially improving DG accuracies in national coordinates. However, simulation results also indicated that the residuals of these methods cannot be entirely neglected. By analyzing the equation derivations of previous map projection correction algorithms, it can be found that their performance is not fully satisfied for two main reasons: (1) the map projection distortion model used is not very accurate, e.g., the angle distortion (it contains three parts: the skew-normal distortion, the normal-section-to-geodesic distortion, and the arc-to-chord distortion. For more details please see Zhang and Shen (2013a)) is not considered in previous studies; (2) an average terrain elevation is adopted in widely used non-iterative earth-curvature-correction methods to approximate real ground heights.

In this paper, we present a new map projection correction method for the high-precision DG of aerial imagery in national coordinates. Different from previous studies, ground coordinates in the Cartesian space are explicitly estimated in our algorithm, and an accurate map projection distortion model can then be adopted and the ground height approximation can also be avoided.

The remainder of this paper is organized as follows. In Section 2, we introduce some background on the DG problem. Then, Section 3 presents our new map projection correction method. Finally, we provide experimental results and conclude the paper in the last two sections.

2. Geometric basis

2.1. Differences between direct georeferencing of imagery and LiDAR data

If technical details not required for this solution, such as the calibration parameters of imaging sensors and the mounting parameters between different sensors (i.e., lever arms and boresight angles), are ignored, the DG models of aerial imagery and airborne LiDAR data in a Cartesian frame can be written as

$$\boldsymbol{T}_{\text{grd}}^{\text{img}} = \boldsymbol{T}_{\text{eo}} + \boldsymbol{T}_{\text{dg}}^{\text{img}} = \boldsymbol{T}_{\text{eo}} + s\boldsymbol{R}_{\text{eo}}\boldsymbol{T}_{\text{sensor}}^{\text{img}} \tag{1}$$

and

$$\boldsymbol{T}_{\text{grd}}^{\text{LiDAR}} = \boldsymbol{T}_{\text{eo}} + \boldsymbol{T}_{\text{dg}}^{\text{LiDAR}} = \boldsymbol{T}_{\text{eo}} + \boldsymbol{R}_{\text{eo}}\boldsymbol{T}_{\text{sensor}}^{\text{LiDAR}} \tag{2}$$

respectively. The superscripts img and LiDAR refer to optical image data and LiDAR data, respectively; $\boldsymbol{T}_{\text{grd}}$ represents the column vector constituted by a ground coordinate; $\boldsymbol{T}_{\text{eo}}$ and $\boldsymbol{R}_{\text{eo}}$ refer to the 3D vector and 3×3 rotation matrix formed by linear and angular EOPs, respectively; $\boldsymbol{T}_{\text{dg}}$ refers to the DG vector (Zhang and Shen, 2013a); s is the scale factor of a bundle ray; and $\boldsymbol{T}_{\text{sensor}}$ is the sensor observation vector and can be given by

$$\boldsymbol{T}_{\text{sensor}}^{\text{img}} = \begin{bmatrix} x \\ y \\ -f \end{bmatrix} \tag{3}$$

and

$$\boldsymbol{T}_{\text{sensor}}^{\text{LiDAR}} = \boldsymbol{R}_{\text{scan}} \begin{bmatrix} 0 \\ 0 \\ -r \end{bmatrix} \tag{4}$$

for aerial images and airborne LiDAR data, respectively, where (x, y) is the image coordinate, f is the focal length, r is the range observation, and $\boldsymbol{R}_{\text{scan}}$ refers to the scan angle matrix (Baltsavias, 1999).

By comparing Eqs. (1) with (2), it can be seen that either the DG process of aerial images or airborne LiDAR data can be expressed as an addition operation between the vectors $\boldsymbol{T}_{\text{eo}}$ and $\boldsymbol{T}_{\text{dg}}$. However, since a camera does not possess range measurement capability like a LiDAR instrument, $\boldsymbol{T}_{\text{dg}}$ cannot be directly derived from the information in a single image.

2.2. Direct georeferencing in national coordinates

The DG model in a national map projection frame can be written as

$$\boldsymbol{T}'_{\text{grd}} = \boldsymbol{T}_{\text{eo}} + \boldsymbol{T}_{\text{dg}} + \Delta(\boldsymbol{T}_{\text{eo}}, \boldsymbol{T}_{\text{dg}}) = \boldsymbol{T}_{\text{grd}} + \Delta(\boldsymbol{T}_{\text{eo}}, \boldsymbol{T}_{\text{dg}}) \tag{5}$$

where $\boldsymbol{T}'_{\text{grd}}$ and $\boldsymbol{T}_{\text{grd}}$ refer to the ground coordinates in the national map projection frame and in the Cartesian space, respectively; Δ refers to the map projection distortion, which is a very complicated function of $\boldsymbol{T}_{\text{eo}}$ and $\boldsymbol{T}_{\text{dg}}$ (Zhang and Shen, 2013a) and is schematically shown by the coordinate difference between G (G_1 or G_2) and G′ in Fig. 1.

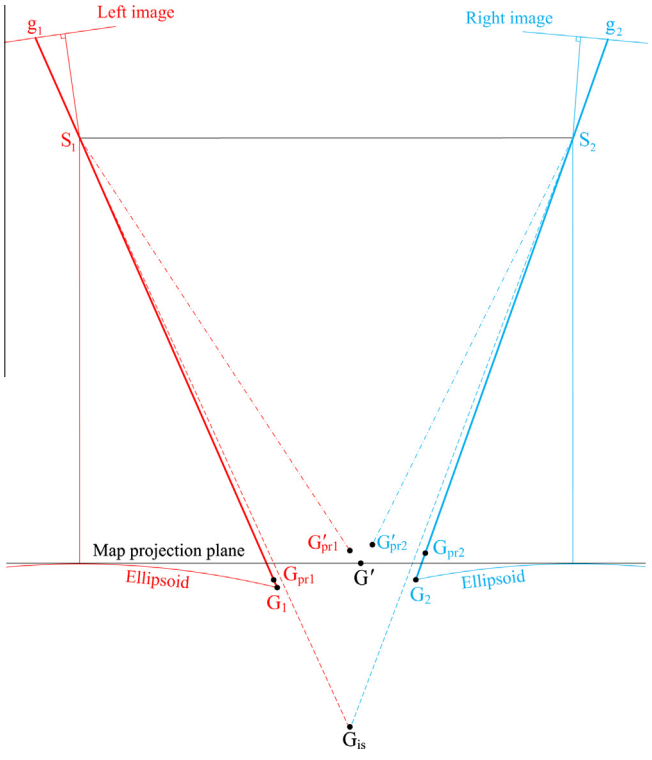

Fig. 1. A two-view geometry in a national map projection frame. G′ is a ground point in national coordinates, and G_1 and G_2 are the corresponding ground positions in the Cartesian space with respect to the perspective centers S_1 and S_2, respectively, where the subscripts 1 and 2 refer to the left and right images, respectively; G_{pr1} and G_{pr2} are the predicted ground positions in the Cartesian space, and G'_{pr1} and G'_{pr2} are their corresponding map projection positions, respectively; G_{is} is the result of a space intersection in national coordinates without correcting any map projection distortions; and g_1 and g_2 are the image points in the left and right images, respectively.

As previously discussed in Section 2.1, the only important difference between the DG models of aerial imagery and airborne LiDAR data is whether $\boldsymbol{T}_{dg}$ is known. Therefore, supposing $\boldsymbol{T}_{dg}$ could be accurately estimated in the data processing of aerial images, all the map projection distortion models and correction equations developed for the DG of airborne LiDAR data in national coordinates can be easily applied. Further, it can be seen from Eq. (1) that the solving of $\boldsymbol{T}_{dg}$ is actually equivalent to calculate $\boldsymbol{T}_{grd}$ because $\boldsymbol{T}_{eo}$ is always known in the DG process.

3. Method description

Our proposed map projection correction method comprises three steps as follows.

(1) Predicting ground point coordinates in Cartesian space.

The ground point in Cartesian space can be predicted from the result of a rough intersection in national coordinates. According to Konecny (2014), the space intersection equation can be written as

$$\boldsymbol{T}_{is}=\begin{bmatrix}X_{is}\\Y_{is}\\Z_{is}\end{bmatrix}=\boldsymbol{T}_{eo1}+s_1\begin{bmatrix}u_1\\v_1\\w_1\end{bmatrix}=\boldsymbol{T}_{eo1}+\frac{(X_{S2}-X_{S1})w_2-(Z_{S2}-Z_{S1})u_2}{u_1w_2-w_1u_2}\begin{bmatrix}u_1\\v_1\\w_1\end{bmatrix} \tag{6}$$

with

$$\begin{bmatrix}u_1\\v_1\\w_1\end{bmatrix}=\boldsymbol{R}_{eo1}\begin{bmatrix}x_1\\y_1\\-f\end{bmatrix} \tag{7}$$

and

$$\begin{bmatrix}u_2\\v_2\\w_2\end{bmatrix}=\boldsymbol{R}_{eo2}\begin{bmatrix}x_2\\y_2\\-f\end{bmatrix} \tag{8}$$

where (X_S, Y_S, Z_S) is the national coordinate of the perspective center S (e.g., S_1 and S_2 in Fig. 1), the subscripts 1 and 2 refer to two different images in a multiple-view geometry. If a ground point is imaged at more than two stations, only two arbitrary images are used in Eq. (6). It should be mentioned that the Z coordinate in our paper refers to an ellipsoidal height as in many previous studies (Legat, 2006; Zhang and Shen, 2013a), though, in practice, orthometric heights are actually used for national mapping.

From simulation results we observed that if the space intersection is directly performed in national coordinates, the intersection result G_{is} never coincides with G' (because all map projection distortions are not corrected), and the coordinate discrepancy between these two points is commonly more significant on the height component than the planimetric component, which is schematically illustrated in Fig. 1. Given that the planimetric coordinate difference between G and G' is mainly caused by the length distortion (Zhang and Shen, 2013a), we can predict the ground position in Cartesian space partly from the following constraint.

$$k_{ld}\sqrt{(X_{pr}-X_S)^2+(Y_{pr}-Y_S)^2}=\sqrt{(X_{is}-X_S)^2+(Y_{is}-Y_S)^2} \tag{9}$$

where (X_{pr}, Y_{pr}) is the planimetric coordinate of the predicted ground point G_{pr} (e.g., G_{pr1} and G_{pr2} in Fig. 1), and k_{ld} refers to the length distortion scale factor and can be given by (Legat, 2006; Zhang and Shen, 2013a)

$$k_{ld}=\frac{kR}{R+h_S+Z_{dg}}\approx\frac{kR}{R+Z_{is}} \tag{10}$$

where R and k are the mean radius of curvature and point scale factor at the perspective center, respectively. For the most widely used transverse Mercator projection, k can be given by (Bomford, 1980)

$$k=k_0\left(1+\frac{X_S^2}{2k_0^2R^2}+\frac{X_S^4}{24k_0^4R^4}\right) \tag{11}$$

where k_0 is the point scale factor at the central meridian, and X_S refers to the east coordinate of the perspective center (not including the false easting).

The second constraint added to the predicted ground point G_{pr} is that it should be located on the light ray in Cartesian space. Consequently, it meets

$$\begin{aligned}\frac{X_{pr}-X_S}{Z_{pr}-Z_S}&=\frac{u}{w}\\\frac{Y_{pr}-Y_S}{Z_{pr}-Z_S}&=\frac{v}{w}\end{aligned} \tag{12}$$

Combining Eqs. (9) and (12) can determine the three unknowns (X_{pr}, Y_{pr}, Z_{pr}) .

(2) Calculating map projection corrections.

For each predicted ground point G_{pr}, map projection corrections are calculated and added to the coordinate of G_{pr}, and the result is denoted as G'_{pr} (see Fig. 1).

This step is exactly the same as the map projection correction process for the DG of airborne LiDAR data in national coordinates, and all equations needed have been derived by Legat (2006) and Zhang and Shen (2013a).

(3) Fine intersection.

As schematically shown in Fig. 1, since the ground point prediction in the first step cannot be very accurate, G'_{pr} commonly does not exactly coincide with G'. However, from simulation results we observed that G'_{pr} is typically substantially located on the line SG', and we can therefore write the following equation.

$$\begin{bmatrix}X'-X_S\\Y'-Y_S\\Z'-Z_S\end{bmatrix}=s_{pr}\begin{bmatrix}X'_{pr}-X_S\\Y'_{pr}-Y_S\\Z'_{pr}-Z_S\end{bmatrix} \tag{13}$$

where (X', Y', Z') is the ground coordinate in the national map projection frame to be solved, and s_{pr} is a scale factor. By eliminating s_{pr} and arranging the terms, Eq. (13) can be further converted to

$$\begin{bmatrix}Z'_{pr}-Z_S & 0 & X_S-X'_{pr}\\0 & Z'_{pr}-Z_S & Y_S-Y'_{pr}\end{bmatrix}\begin{bmatrix}X'\\Y'\\Z'\end{bmatrix}=\begin{bmatrix}Z'_{pr}-Z_S & 0 & X_S-X'_{pr}\\0 & Z'_{pr}-Z_S & Y_S-Y'_{pr}\end{bmatrix}\begin{bmatrix}X_S\\Y_S\\Z_S\end{bmatrix} \tag{14}$$

In Eq. (14), two linear equations are obtained from one image, and at least two conjugate image points are therefore required to solve the three unknowns by an intersection.

4. Experiments

4.1. Schemes

Table 1 lists the five map projection correction schemes that were tested in the experiments.

Table 1
Map projection correction schemes.

ID	Scheme	Description
TR	Traditional correction method	This scheme employs the previous best map projection correction method, in which the earth curvature and length correction algorithms were developed by Zhao et al. (2014) and Zhang and Shen (2013b), respectively
TRit	Traditional correction method using an iterative earth curvature correction algorithm	This scheme is the same as the last one except the earth curvature correction algorithm is modified to be suitable for mountainous regions by adopting an iterative strategy suggested by Wang (1980)
Ntr	Our new method using the traditional map projection distortion model	The map projection correction equations used in the second step of our method were first derived by Legat (2006)
Npr	Our new method using the practical map projection distortion model	This scheme is the same as the last one except that the map projection correction equations used were first given in Section 3.2 of Zhang and Shen (2013a)
Nhi	Our new method using the high-precision map projection distortion model	This scheme is the same as the last two except that the map projection correction equations used were first given in Section 3.1 of Zhang and Shen (2013a)

4.2. Data

As with many previous studies (Legat, 2006; Zhang and Shen, 2013b; Zhao et al., 2014), simulated data were used in this paper to evaluate the performance of different map projection correction schemes. As listed in Table 2, six scenarios were simulated. In each scenario, the block included five flight strips, each of which comprised of five images. The geographic coordinate of the first perspective center was (30°N, 120°E). In the cover area of a single image, 10,000 evenly distributed ground points were simulated.

In the first four scenarios (A1–A3 and B), a Leica RC30 camera was used. Its focal length was 153 mm, and the frame size was 230 mm × 230 mm. The forward and side overlaps were set to 60% and 30%, respectively. As shown in Table 2, scenario A1 simulated an ideal flight and terrain condition (i.e., all photographs were vertically imaged and exposed at designed positions, and the terrain was flat); scenario A2 added random noise to ground elevations to simulate terrain undulations; scenario A3 simulated a realistic flight condition by adding maximums of 10 m and 5° random values to the linear and angular EOPs, respectively; and scenario B simulated an extreme case of a high flight height and large terrain undulations.

In the last two scenarios (C1 and C2), a Leica RCD30 oblique camera was used, and its look angle and focal length were 35° and 50 mm, respectively. The image size was 8956 × 6708 pixels, and the pixel size was 6 μm. The forward and side overlaps were set to 80% and 60%, respectively. As shown in Table 2, the only difference between scenarios C1 and C2 is that the latter added a maximum of 200 m random values to ground heights.

Table 2
Simulated scenarios.

Scenario	View	Flight height above ground (m)	Maximum deviation from the normal case		
			Linear EOPs (m)	Angular EOPs (deg)	Ground height (m)
A1	Nadir	2000	0	0	0
A2	Nadir	2000	0	0	200
A3	Nadir	2000	10	5	200
B	Nadir	8000	10	5	800
C1	Oblique	2000	10	5	0
C2	Oblique	2000	10	5	200

Table 3
Technical characteristics of the national map projection frame in the experiments.

Category	Parameter	Value	Unit
7-parameter from WGS 84 datum to national datum	Scale factor	1.00005	–
	Translation vector	(370.9492, 282.6227, −4.7778)	m
	Rotation angles	(−0.0014, 0.0022, −0.0025)	deg
Ellipsoid	Type	Krassovsky	–
Map projection	Type	Universal transverse Mercator (UTM)	–
	Central meridian	117	deg

Table 3 shows the definition of the national map projection frame used in the experiments. The datum transformation parameters originate from a real airborne laser scanning project, but some insignificant digits were rounded off.

4.3. Results and analysis

Table 4 shows the experimental results of the first three simulated scenarios (A1–A3). In scenario A1, schemes TR, TRit, and Ntr yielded similar results, and schemes Npr and Nhi provided much better accuracy. This is caused by the different map projection distortion models used in these correction schemes. Schemes TR, TRit, and Ntr employed the traditional distortion model, which only deals with the earth curvature and length distortions (Legat, 2006). Scheme Npr or Nhi, on the other hand, adopted a more accurate distortion model (the practical or high-precision model, respectively; the differences between these models can be found in Zhang and Shen, 2013a), in which more types of map projection distortions (e.g., the arc-to-chord distortion) are considered and more rigorous earth curvature and length correction equations are used (Zhang and Shen, 2013a).

Comparing the results of scenario A2 with those of A1, we found that the performance of scheme TR was significantly degraded, while the accuracy of scheme TRit and our proposed method (schemes Ntr, Npr, and Nhi) basically remained the same. In scheme TR, the earth curvature correction algorithm used was developed by Zhao et al. (2014), and it employed the average terrain elevation in calculation. Thus, if a ground point is more away from the average terrain plane, the correction accuracy of Zhao et al.'s method will get worse. By adopting an iterative strategy, scheme TRit can use real ground heights to compute earth curvature corrections, and its performance is therefore nearly not degraded in mountainous regions. Our proposed method explicitly estimates ground positions in the Cartesian space and then calculates earth curvature distortions as well as other map projection distortions. Its accuracy, therefore, is also rarely influenced by terrain undulations.

In scenario A3, which simulated a more realistic data acquisition condition, the errors of scheme TR mainly appear in the height component and can be up to 7 cm. The performance of scheme TRit and our proposed method is much better. When the practical or high-precision map projection distortion model (schemes Npr or Nhi) was used, the maximum residual of our new method is only slightly larger than or smaller than 1 mm, respectively.

As shown in Table 5, in scenario B (an extreme case of a high flight height and large terrain undulations), the residuals of scheme Nhi are only several centimeters, while the maximum error of

Table 4
Error statistics of direct georeferencing with flying height of 2000 m above ground.

Scenario	Scheme	RMS (mm)		Max. Dev. (mm)	
		Plane	Height	Plane	Height
A1 (no terrain undulations)	TR	5.5	5.5	13.9	−21.9
	TRit	5.5	5.5	13.9	−21.8
	Ntr	3.8	6.8	13.9	22.6
	Npr	0.5	0.8	1.2	−1.5
	Nhi	0.0	0.0	0.1	0.2
A2 (a mountainous case)	TR	5.6	10.4	20.6	−57.6
	TRit	5.5	5.6	15.5	26.1
	Ntr	3.8	7.0	15.5	27.0
	Npr	0.4	0.8	1.3	−1.5
	Nhi	0.0	0.0	0.1	0.2
A3 (a more realistic case)	TR	5.9	11.3	27.2	−66.1
	TRit	5.7	5.9	19.9	28.9
	Ntr	4.1	7.7	19.4	30.0
	Npr	0.4	0.7	1.5	−1.6
	Nhi	0.0	0.0	0.2	0.3

Table 5
Error statistics of direct georeferencing with flying height of 8000 m above ground.

Scenario	Scheme	RMS (mm)		Max. Dev. (mm)	
		Plane	Height	Plane	Height
B (an extreme case)	TR	96.5	182.6	582.7	−1179.5
	TRit	93.8	93.5	311.1	−502.7
	Ntr	67.6	122.5	309.9	−491.8
	Npr	2.0	3.7	13.5	28.6
	Nhi	0.8	1.3	12.0	−21.8

Table 6
Error statistics of direct georeferencing results in two oblique imaging scenarios.

Scenario	Scheme	RMS (mm)		Max. Dev. (mm)	
		Plane	Height	Plane	Height
C1 (no terrain undulations)	TR	21.9	7.2	85.4	−53.1
	TRit	21.9	7.1	85.0	−52.3
	Ntr	21.3	12.3	56.5	−27.1
	Npr	1.7	1.7	6.0	−5.9
	Nhi	0.1	1.0	1.5	6.5
C2 (a mountainous case)	TR	53.5	63.4	544.6	−399.6
	TRit	22.9	9.7	104.3	56.8
	Ntr	22.7	12.7	68.8	36.5
	Npr	1.9	1.7	7.0	−5.9
	Nhi	0.2	1.0	1.8	6.3

scheme TR exceeds 1 m. As a comparison, when the same high-precision map projection distortion model is used, the DG errors of airborne LiDAR data in a similar simulated scenario can be less than 1 mm (Zhang and Shen, 2013a), which indirectly proves that the correction errors of scheme Nhi were mainly caused by the imperfect ground point prediction process. Although there are certainly some ways to further improve the ground prediction accuracy, we are satisfied with the current algorithm because the correction residuals are already much smaller than most of the errors in the direct georeferencing (e.g., errors in POS data).

Table 6 shows the experimental results of two oblique imaging scenarios. Comparing the results of scenarios C1 and C2 with those of A1 and A2, we found that the performance of scheme TR is much more sensitive to terrain undulations in an oblique imaging geometry than that in a vertical imaging condition (the maximum error of scheme TR in scenario C2 was almost ten times larger than that in scenario C1, while the maximum error in scenario A2 was only two times of that in scenario A1). The geometric explanation

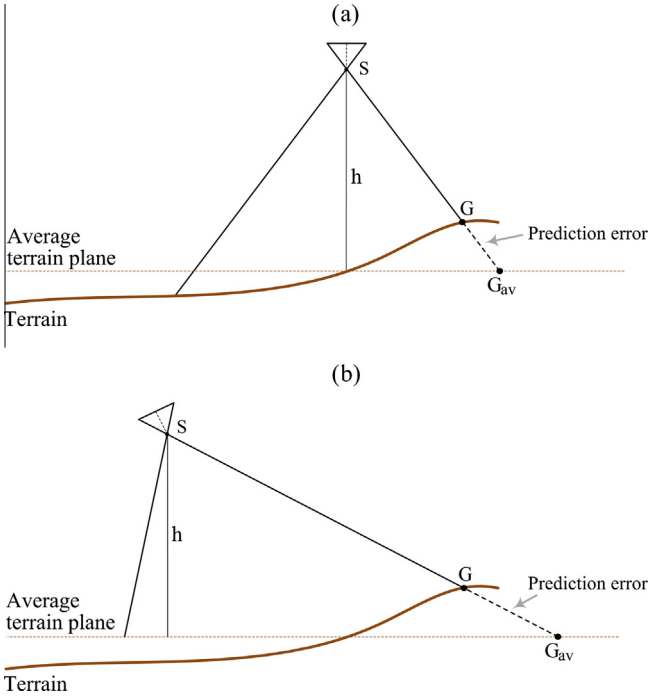

Fig. 2. The impact of terrain undulations on the ground point prediction results in Zhao et al.'s earth curvature correction method. (a) Vertical and (b) oblique imaging geometry conditions. G is a ground point, and G_{av} is the predicted ground position by means of an average terrain plane.

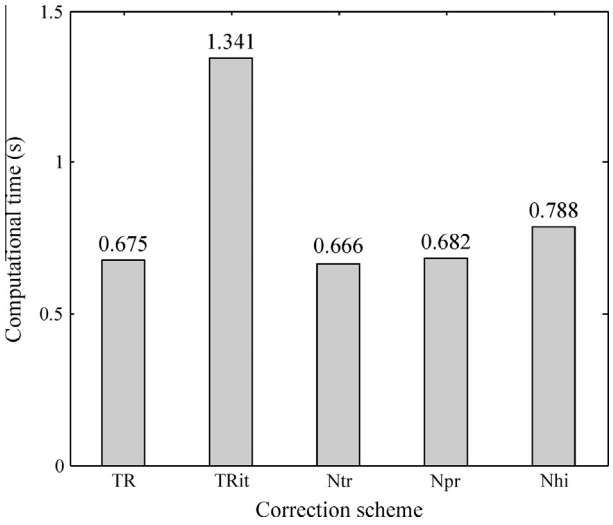

Fig. 3. Computational costs of direct georeferencing experiments in scenario B. The test program ran on an Intel Core i3 M 330 processor and was compiled with Intel C/C++ 12.0 compiler. In the iterative earth curvature correction algorithm of scheme TRit, the convergence threshold for the height difference between two iterative ground points was set to 1 cm, and only two ground points were used in the intersection of the first iteration to save computational time.

for this is illustrated in Fig. 2. In Zhao et al.'s earth curvature correction method, as an average terrain elevation is adopted to approximate real ground heights, the earth curvature correction is actually calculated from the vector SG_{av} (G_{av} is the intersection point between the light ray and the average terrain plane), but not SG. When the same terrain undulations are encountered, the prediction error (i.e., the distance between G_{av} and G) in an oblique imaging scenario is commonly much larger than that in a vertical imaging scenario, and the map projection correction error is therefore considerably bigger because the earth curvature distortion is a

quadratic function of the planimetric length of a DG vector (Zhang and Shen, 2013a). Our proposed method (schemes Ntr, Npr, and Nhi), on the other hand, is not substantially influenced by terrain undulations in an oblique imaging geometry, because the predicted ground point G_{pr} is always very close to the actual ground point G in the Cartesian space (see Fig. 1).

Computational efficiency is also of importance to evaluate different map projection correction methods. As shown in Fig. 3, since an iterative earth curvature correction algorithm was used, scheme TRit needs much more computational time than scheme TR. When the traditional or practical map projection distortion model is adopted, the computational cost of our method (i.e., scheme Ntr or Npr) is close to that of scheme TR, and when the high-precision distortion model is used, our method (i.e., scheme Nhi) requires considerably more computing time. Given that the correction accuracy of scheme Nhi is only slightly better than that of scheme Npr (see Tables 4–6), the latter is more recommend for practical use.

5. Conclusions

This paper presented a new map projection correction method for the direct georeferencing of aerial images in national coordinates. Unlike previous correction algorithms, our new method explicitly estimates ground positions in the Cartesian space, and it can therefore directly use the accurate map projection correction equations that were derived for the direct georeferencing of airborne LiDAR data in national coordinates in earlier studies. Simulation results prove that our new method can safely replace previous methods because when the practical map projection distortion model is used, the accuracy of our method is by one order of magnitude better than the previous best approach, while their computational efforts are at the same level.

Acknowledgments

This work was supported in part by the National Natural Science Foundation of China under Grants 41322010 and 41171292, and the National Hi-Tech Research and Development Program with project number 2013AA12A401.

References

Baltsavias, E.P., 1999. Airborne laser scanning: basic relations and formulas. ISPRS J. Photogramm. Remote Sens. 54 (2–3), 199–214.
Bomford, G., 1980. Geodesy, fourth ed. Clarendon Press, Oxford.
Cramer, M., Kresse, W., Skaloud, J., Haala, N., Nittel, S., Wallgrün, J.O., 2012. Data capture. In: Kresse, W., Danko, D.M. (Eds.), Handbook of Geographic Information. Springer, Heidelberg, pp. 211–301.
Kraus, K., 2007. Photogrammetry: Geometry from Images and Laser Scans, second ed. Walter de Gruyter, Berlin.
Konecny, G., 2014. Geoinformation: Remote Sensing, Photogrammetry and Geographic Information Systems, second ed. CRC Press, Baca Raton.
Legat, K., 2006. Approximate direct georeferencing in national coordinates. ISPRS J. Photogramm. Remote Sens. 60 (4), 239–255.
Mikhail, E.M., Bethel, J.S., McGlone, J.C., 2001. Introduction to Modern Photogrammetry. John Wiley & Sons, New York.
Mugnier, C.J., Förstner, W., Wrobel, B., Paderes, F., Munjy, R., 2004. The mathematics of photogrammetry. In: McGlone, J.C., Mikhail, E.M., Bethel, J.S., Mullen, R. (Eds.), Manual of Photogrammetry, fifth ed. American Society for Photogrammetry and Remote Sensing, Bethesda, pp. 181–316.
Ressl, C., 2001. The impact of conformal map projections on direct georeferencing. Int. Arch. Photogramm. Remote Sens. Spatial Inf. Sci. 34 (Part B), 283–288.
Skaloud, J., 2002. Direct georeferencing in aerial photogrammetric mapping. Photogramm. Eng. Remote Sens. 68 (3), 207–210.
Skaloud, J., Legat, K., 2008. Theory and reality of direct georeferencing in national coordinates. ISPRS J. Photogramm. Remote Sens. 63 (2), 272–282.
Wang, S.C., 1980. Einfluß der geodätischen Abbildungsverzerrungen auf die photogrammetrische Punktbestimmung. Ph.D. thesis. Deutsche Geodätische Kommission, München, Germany, 162p (in German).
Wang, Z., 1990. Principles of Photogrammetry (with Remote Sensing). Press of Wuhan Technical University of Surveying and Mapping, Publishing House of Surveying and Mapping, Beijing, China.
Yastikli, N., Jacobsen, K., 2005a. Direct sensor orientation for large scale mapping—Potential, problems, solutions. Photogramm. Rec. 20 (111), 274–284.
Yastikli, N., Jacobsen, K., 2005b. Influence of system calibration on direct sensor orientation. Photogramm. Eng. Remote Sens. 71 (5), 629–633.
Zhang, Y., Shen, X., 2013a. Direct georeferencing of airborne LiDAR data in national coordinates. ISPRS J. Photogramm. Remote Sens. 84, 43–51.
Zhang, Y., Shen, X., 2013b. Approximate correction of length distortion for direct georeferencing in map projection frame. IEEE Geosci. Remote Sens. Lett. 10 (6), 1419–1423.
Zhao, H., Zhang, B., Wu, C., Zuo, Z., Chen, Z., Bi, J., 2014. Direct georeferencing of oblique and vertical imagery in different coordinate systems. ISPRS J. Photogramm. Remote Sens. 95, 122–133.